Pair processes in $CsCdBr_3:Er^{3+}$: A study by up-conversion and excited-state absorption of efficient uv and blue anti-Stokes emissions

F. Pellé and Ph. Goldner
Laboratoire de Physico-Chimie des Matériaux, 1, Place Aristide Briand, 92190 Meudon Bellevue, France
(Received 19 March 1993)

Excitation in the $^4S_{3/2}$, $^4F_{7/2}$, or $^4F_{5/2}$ levels results in efficient anti-Stokes emissions between 25 300 and 32 600 cm^{-1}. Up-conversion is due to an energy transfer in symmetric pairs, which are the dominant center in this compound. To determine transfer rates for this mechanism, transients of $^4D_{5/2}$ and $^4G_{9/2}$ levels have been studied using excited-state absorption in the $^4F_{9/2}$ state. Detailed excitation spectra have also been recorded for these high-energy levels. A close examination of fluorescence dynamics for these various excitation paths showed the importance of competing pair relaxations in this system.

I. INTRODUCTION

Energy transfer between ions in dimers or larger aggregates can be very efficient in rare-earth-doped compounds. Especially, anti-Stokes emissions can be obtained by the interaction of several simultaneously excited ions. This phenomenon has been demonstrated in many compounds where isolated ions are the dominant centers.[1–6] In this case up-conversion can be used to identify aggregate excitation and emission lines. Indications on the nature of the energy transfer can also be deduced from the variation of the transfer rate with interionic distance.[7] New, compact, diode-pumped, up-conversion lasers could also be based on this process for such laser operation has only been demonstrated in hosts with a random distribution of rare-earth dopants.[8]

$CsCdBr_3$ which belongs to the AMX_3 family has the hexagonal structure of $CsNiCl_3$. This crystal is a very interesting matrix for such studies because trivalent impurities enter this host nearly only as charge compensated complexes.[9,10] Two dimers can be observed in $CsCdBr_3:M^{3+}$. The first one involves two equivalent ions separated by a vacancy (M^{3+}-vacancy-M^{3+}). The distance between them is about 6 Å. Apart from this dimer a small number of nonsymmetric pairs (M^{3+}-M^{3+}-vacancy) is also found. In these complexes the crystal field for the central ion is very close to the one for ions in symmetric pairs. The other ion has levels slightly apart from the first one. An energy transfer between these nonequivalent centers has also been observed for Nd^{3+}- and Er^{3+}-doped samples.[11,12] Up-conversion is usually found to occur from doubly excited pairs for symmetric dimers in rare-earth-doped $CsCdBr_3$, for example, with Pr^{3+},[13] Ho^{3+},[14] Tm^{3+},[15] Er^{3+}.[16–18,12]

Dynamics of these emissions can also be studied especially to evaluate the up-conversion transfer rates. In this case, it is usually necessary to measure independently the lifetime of the highest emitting level which should exhibit the simplest behavior in up-conversion. For infrared excitations, emissions corresponding to two-photon absorption come from levels easily excited by visible emitting sources. But when excitation energy lies itself between 450 and 550 nm, levels of energy as high as 38 000 cm^{-1} can be easily reached through up-conversion. Direct excitation in this region is more complex and requires frequency laser doubling or UV sources.[17,19] Another possibility is to use again an up-conversion process: two tunable dye lasers operating in the visible region can achieve excited-state absorption (ESA). We found this last method efficient enough to allow detailed excitation and emission spectra of high-lying levels to be recorded along with the fluorescence transients for $CsCdBr_3:Er^{3+}$.

Decay analysis is also difficult because of the several relaxations possible from a pair state. For example, Tallant, Miller, and Wright[20] showed in CaF_2 that cross relaxation could compete efficiently with multiphonon relaxation in Er^{3+} dimers. In this case the addition of several processes yields to decay curves very different from those expected from single-ion relaxations. For anti-Stokes emissions the same kind of competition between mechanisms can occur to populate a given state. These emission transients depend therefore strongly on the initial pair state.

In this paper, we present results on emissions from the $^4G_{9/2}$, $^4G_{11/12}$, and $^4D_{5/2}$ levels obtained under various excitations. First, site selection with excitation in the $^4F_{7/2}$ level confirmed the nature of the up-conversion process. ESA then provided details on the energies of the $^4D_{5/2}$ and $^4G_{9/2}$ sublevels. Finally a detailed description of the dynamics of the most intense anti-Stokes emissions is given for the different excitations.

II. EXPERIMENT

Experiments were performed on a monocrystal grown by the Bridgman method under a bromine atmosphere after drying of the starting products. The nominal Er^{3+} concentration of the sample was 0.1%.

A CTI Cryogenics cryostat cooled the sample down to 10 K. All spectra and transients were recorded at this temperature. Luminescence was analyzed by a Jobin-Yvon HR1000 spectrometer and an RCA 56 TVP or a cooled Hamamatsu R628 photomultiplier. Appropriate filters were used to suppress scattered laser light.

0163-1829/93/48(14)/9995(16)/$06.00

Fluorescence transients were recorded by a Tektronix 7912AD digitizer interfaced with a PC-AT microcomputer.

CW excitations were provided by a Coherent Innova 300 argon laser pumping DCM dye in a 590 dye laser with 0.06-nm bandwidth. A nitrogen pulsed laser Sopra 2001 pumped a Molectron dye laser to produce excitation between 548 and 370 nm with coumarin 485, 481, 460, and BBQ dyes (0.08-nm bandwidth). The experimental setup for ESA experiments is presented in Fig. 1. Low-power UV excitation was generated by a 150W XBO Xenon lamp filtered by a Jobin-Yvon HD10 double monochromator.

III. UP-CONVERSION LUMINESCENCE

A. Doubly excited dimers

Excitation in the $^4F_{7/2}$ level at 20 347 cm^{-1} [corresponding to the $^4I_{15/2}(1) \rightarrow {}^4F_{7/2}(2)$ transition] yields to strong anti-Stokes emissions between 25 300 and 32 600 cm^{-1}. Seven emission regions are observed between 307 and 311 nm [Fig. 2(a)], 317 and 323 nm [Fig. 2(b)], 335 and 339.5 nm [Fig. 2(c)], 359.5 and 361.5 nm [Fig. 2(d)], 365 and 375 nm [Fig. 2(e)], 382 and 390 nm [Fig. 2(f)], and between 390 and 395 nm [Fig. 2(g)]. In order to determine the nature of this fluorescence, variation of the emission intensities versus excitation power was studied. Each observed emission showed a quadratic dependence on the pump beam intensity which corresponds to a two-photon process. Figure 3 shows the experimental data obtained for *C*, *B*, and *F* emissions.

All observed anti-Stokes emissions present the same excitation spectrum which consists of two peaks at 20 347 and 20 393 cm^{-1} [Fig. 4 curve (b)]. A previous study[12] carried out on several Er^{3+}-doped and Er^{3+}-Yb^{3+}-codoped $CsCdBr_3$ samples allowed us to identify by site selection the two charge-compensated dimers possible in this matrix (see the Introduction). This was performed by analyzing the $^4S_{3/2} \rightarrow {}^4I_{15/2}$ transition with excitation in the $^4F_{7/2}$ level. In the nonsymmetric dimers, the central ion levels are extremely close to those of Er^{3+} in symmetric complexes and slightly apart from the other ion of the pair. Moreover, a strong energy transfer couples the ions of nonsymmetric complexes so that excitation spectra of the $^4S_{3/2}$ emission always include lines from the two dimers [Fig. 4 curve (a)]. However, excitation spectra of the anti-Stokes emissions only show the lines corresponding to the symmetric complexes [Fig. 4 curve (b)]. This confirms that this process can only occur in simultaneously excited pairs and is produced by an energy transfer between two ions in the $^4F_{7/2}$ state.

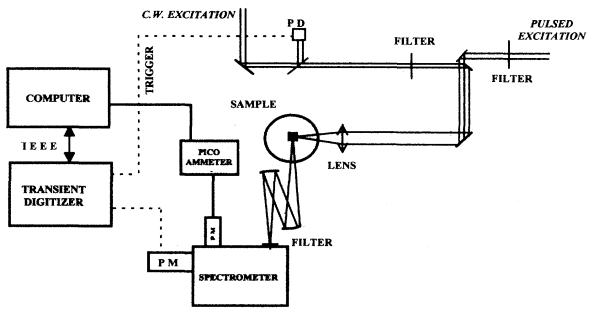

FIG. 1. Experimental setup for excited-state absorption experiments.

If one ion transfers all its energy to its neighbor during the up-conversion process, the level reached is the $^2I_{11/2}$ state, lying at 40 800 cm^{-1} above the ground state in $CsMgCl_3$.[19] Other articles on energy levels of rare-earth ions confirm this position.[21,22] In the following most of the levels are labeled according to Dieke and Crosswhite.[23] We also used Carnall's notation for some high-energy levels.

Emissions located between 335 and 339.5 and 382 and 390 nm have already been observed in $CsCdBr_3$:Er^{3+} by up-conversion from cw or pulsed excitations in the $^4S_{3/2}$,[16,17] $^4I_{11/2}$, $^4I_{9/2}$,[18,24] and $^4F_{9/2}$ levels.[12] They have been respectively attributed to the $^4G_{9/2} \rightarrow {}^4I_{13/2}$ and the $^4G_{11/2} \rightarrow {}^4I_{15/2}$ transitions. Concerning the other emissions, the large number of Er^{3+} levels allows them to correspond to several transitions. To attribute these emissions more clearly, fluorescence under UV direct excitation has been studied.

B. UV excitation

A xenon lamp filtered by a double monochromator provided direct excitation in the levels located between 26 882 and 40 000 cm^{-1}. Previously observed emissions were recorded under these conditions. Excitation spectra in this region show a few levels (Fig. 5). The fluorescence yield under this excitation is weak and the analysis of these results can only give a first approximation on the average energy of these states [Table I (top)]. A comparison between our values and some published data is presented in Table I (bottom). From these energy positions, observed emissions can be more precisely attributed (Table II). It is worth pointing out that the level of highest energy recorded in emission or excitation is $^4D_{5/2}$. In particular, no emission from the $^2I_{11/2}$ level was observed.

C. Excited-state absorption

We have completed the study of the levels implied in the up-conversion process by ESA measurements because UV experiments could not give the fine structure of these levels due to the poor resolution of the excitation device (6 nm) and their low absorption. The lifetimes of these levels were also necessary for the treatment of the fluorescence transients.

ESA was performed using first a cw excitation from a dye laser in order to populate the $^4F_{9/2}$ levels of Er^{3+}. This excitation, fixed at 15 152.5 cm^{-1}, was resonant with the $^4I_{15/2}(1) \rightarrow {}^4F_{9/2}(2)$ transition which is the most intense absorption to the $^4F_{9/2}$ level. At low excitation power, a stationary state is obtained for the $^4F_{9/2}$ level and levels of lower energies. We maintained a low beam

intensity to avoid strong anti-Stokes emissions from the $^4S_{3/2}$, $^2H_{11/2}$, $^4F_{7/2}$, $^4F_{5/2}$, $^2H_{9/2}$, $^4G_{11/2}$ levels which can be obtained when excitation power is increased.[12] A second excitation, pulsed and tunable, from another dye laser pumped with a nitrogen laser allows absorption from the $^4F_{9/2}$ excited state to be recorded. The energy range between 34 230 and 42 032 cm^{-1} can then be explored using several dyes.

For each excited level, the linear dependence of the emission intensities on the power of each excitation was checked. In particular, no emission could be observed when blocking the red beam. This result confirms the lack of resonance of the pulsed excitation with any transition from the ground state. The measurement of the fluorescence transients of the directly excited levels also confirms the ESA process since these decay curves exhib-

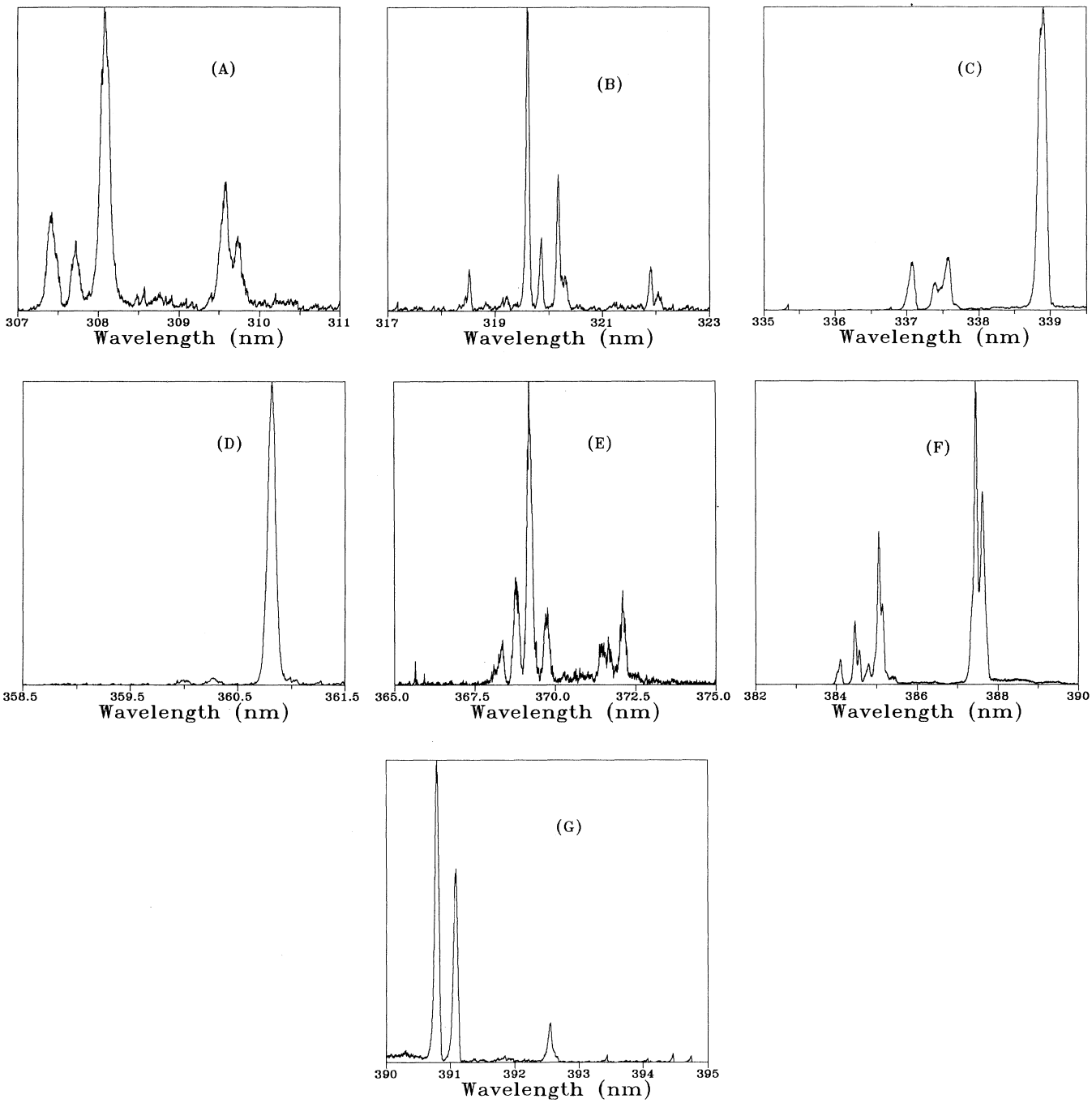

FIG. 2. Emission observed under excitation in the $^4F_{7/2}$ level: (a) $^2P_{3/2}\rightarrow{}^4I_{15/2}$, (b) $^4D_{5/2}\rightarrow{}^4I_{13/2}$, (c) $^4G_{9/2}\rightarrow{}^4I_{13/2}$, (d) $^4D_{5/2}\rightarrow{}^4I_{11/2}$, (e) $^2G_{9/2}\rightarrow{}^4I_{15/2}$, (f) $^4G_{11/2}\rightarrow{}^4I_{15/2}$, and (g) $^4D_{5/2}\rightarrow{}^4I_{9/2}$.

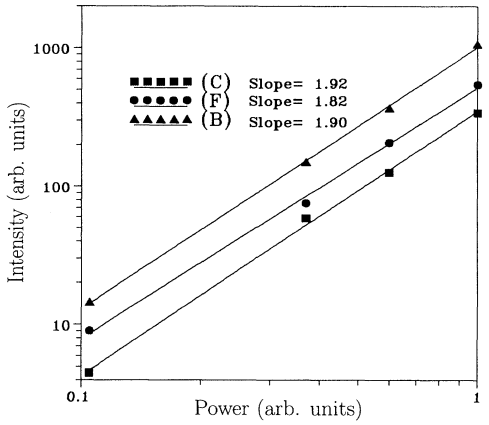

FIG. 3. Power dependence of (*C*), (*F*), and (*B*) up-converted emissions.

it no rise time.

Concerning the two different types of pairs, ESA can excite both of them as in direct excitation experiments and cannot select the symmetric complexes like up-conversion in doubly excited pairs. However, we will assume that the nonsymmetric pairs, which are a minor center, contribute for a small part only in the fluorescence spectra. To ensure that excitation spectra and fluorescence transients also mainly reflect the M^{3+}-vacancy-M^{3+} dimers, a large bandwidth analysis was used.

1. *Excitation in the $^4G_{9/2}$ level*

Er^{3+} ions being excited in the $^4F_{9/2}$ level at 15 152.5 cm^{-1}, the coumarin 481 dye covers the energy range between 34 228 and 36 650 cm^{-1}. In this case, emissions attributed to the $^4G_{9/2}\rightarrow{}^4I_{13/2}$ (*C*) and $^4G_{11/2}\rightarrow{}^4I_{15/2}$ (*F*) transitions are observed with a significant intensity.

$^4F_{9/2}\rightarrow{}^4G_{9/2}$ excitation spectrum monitoring (*C*) emission is shown in Fig. 6. The cw excitation being resonant with the $^4I_{15/2}\rightarrow{}^4F_{9/2}(2)$ transition, the $^4F_{9/2}(1)$ sublevel located at 15 134.2 cm^{-1} (Ref. 16) is also populated by relaxation from $^4F_{9/2}(2)$. The energy gap between these two sublevels (18 cm^{-1}) is therefore found between the lines corresponding to transitions to the same $^4G_{9/2}$ sublevel. Energies of the $^4G_{9/2}$ sublevels are listed in Table III.

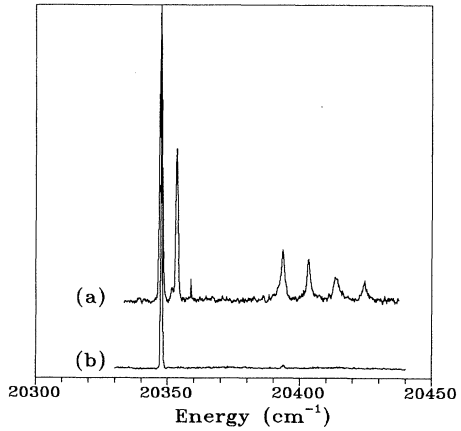

FIG. 4. $^4I_{15/2}\rightarrow{}^4F_{7/2}$ excitation spectra monitoring (*a*) Stokes and (*b*) up-converted emissions.

2. *Excitation in the $^4D_{5/2}$ and $^4D_{7/2}$ levels*

To reach the energy range comprised between 37 130 and 38 680 cm^{-1} coumarin 440 dye was used for pulsed excitation. Under double pumping, the excitation spectrum monitoring the $^4G_{9/2}\rightarrow{}^4I_{13/2}$ emission is presented in Fig. 7. We divide it into five spectral regions.

Between 22 000 and 22 150 cm^{-1}, two excitation peaks observed at 22 017 and 22 019.5 cm^{-1} [Fig. 7(a)] are also observed without red excitation. They do not correspond to an ESA process but to the $^4I_{15/2}\rightarrow{}^4F_{5/2}$ transition. Similarly, the line centered at 22 412.7 cm^{-1} [Fig. 7(b)] is attributed to the $^4I_{15/2}\rightarrow{}^4F_{3/2}$ transition.

The strong excitation lines observed between 22 700 and 23 150 cm^{-1} [Fig. 7(c)] disappear when the pumping in the $^4F_{9/2}$ level is turned off. We attribute these lines to

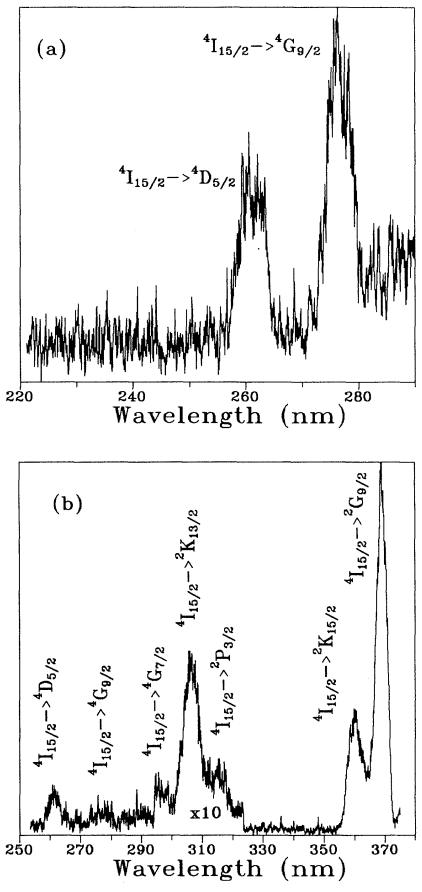

FIG. 5. Excitation spectra obtained under direct UV excitation. (a) monitoring $^4G_{9/2}\rightarrow{}^4I_{13/2}$, (b) monitoring $^4G_{11/2}\rightarrow{}^4I_{15/2}$.

TABLE I. (Top) Observed excitation peaks and corresponding levels monitoring *C* and *F* emissions under direct UV excitation. (Bottom) Energy levels of Er^{3+} in $CsCdBr_3$ in comparison with Er^{3+} levels in other compounds.

Analysis (nm)	Excitation (cm^{-1})	Level
338	38 314	$^4D_{5/2}$
	36 230	$^4G_{9/2}$
387.7	33 784	$^4G_{7/2}$
	32 680	$^2K_{13/2}$
	31 645	$^2P_{3/2}$
	27 777	$^2K_{15/2}$
	27 100	$^2G_{9/2}$

Level	$CsCdBr_3:Er^{3+}$	Er^{3+} (aq) (Ref. 21)	$La_2O_2S:Er^{3+}$ (Ref. 22)
$^2G_{9/2}$	27 100	27 400	27 425
$^2K_{15/2}$	27 777	27 800	
$^2G_{7/2}$		28 000	27 800
$^2P_{3/2}$	31 645	31 600	31 230
$^2K_{13/2}$	32 680	33 200	33 000
$^4G_{5/2}$		33 400	
$^4G_{7/2}$	33 784	34 050	34 081
$^2D_{5/2}$		34 850	34 680
$^4G_{9/2}$	36 266.7	36 550	36 420
$^4D_{5/2}$	38 094.9	38 600	38 365
$^4D_{7/2}$	38 579	39 200	
$^2I_{11/2}$	40 800[a]	41 150	
$^2I_{13/2}$		43 550	

[a]In $CsMgCl_3$ (Ref. 19).

the $^4F_{9/2} \rightarrow {}^4D_{5/2}$ transition because emissions from the $^4D_{5/2}$ level exhibit no rise time under this excitation. The energy of the $^4D_{5/2}$ level deduced from the double pumping (around 38 000 cm^{-1}) is also in agreement with UV excitation. Finally, the energy gap of 18 cm^{-1} corresponding to the separation of the $^4F_{9/2}(2)$ and $^4F_{9/2}(1)$ sublevels is again found in the spectrum. However, analysis of the fluorescence decays showed that excitations at 22 858.8 and 22 876.2 [indicated in Fig. 7(c) by arrows] give a slightly different result than excitation in the

TABLE II. Energies and assignment of anti-Stokes emissions recorded under excitation in the $^4F_{7/2}$ level.

Label	Energy (cm^{-1})	Transition
A	32 573.3–32 154.3	$^2P_{3/2} \rightarrow {}^4I_{15/2}$
B	31 545.7–30 959.7	$^4D_{5/2} \rightarrow {}^4I_{13/2}$
C	29 850.7–29 455.1	$^4G_{9/2} \rightarrow {}^4I_{13/2}$
D	27 816.4–27 662.5	$^4D_{5/2} \rightarrow {}^4I_{11/2}$
E	27 397.3–26 666.7	$^2G_{9/2} \rightarrow {}^4I_{15/2}$
F	26 178.0–25 641.0	$^4G_{11/2} \rightarrow {}^4I_{15/2}$
G	25 641.0–25 316.4	$^4D_{5/2} \rightarrow {}^4I_{9/2}$

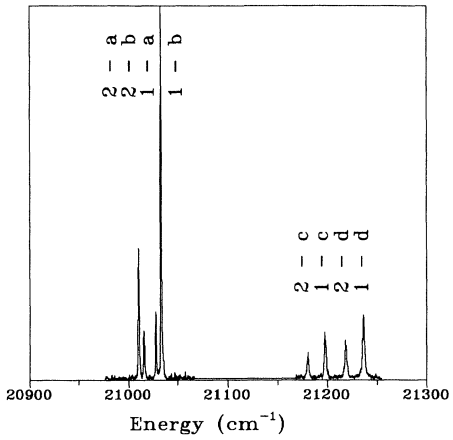

FIG. 6. $^4F_{9/2} \rightarrow {}^4G_{9/2}$ excitation spectra monitoring $^4G_{9/2} \rightarrow {}^4I_{13/2}$ emission. (Transition labels refer to Table III.)

other peaks. We attribute these lines to ions in nonsymmetric pairs. Energies of the $^4D_{5/2}$ sublevels are reported in Table III.

Weak lines between 23 150 and 23 300 cm^{-1} [Fig. 7(c)] have not been clearly identified. They are observed only under double pumping and could correspond to three-photon processes.

Finally, the excitation lines recorded at 23 443.5 and 23 426.6 cm^{-1} [Fig. 7(d)], which are separated by 17 cm^{-1} and due to an ESA process, are attributed to the $^4F_{9/2} \rightarrow {}^4D_{7/2}$ transition. This gives an energy of 38 579 cm^{-1} for the $^4D_{7/2}$ level.

3. *Excitation at higher energy*

We used in this case BBQ dye to excite levels between 40 466 and 42 032 cm^{-1} with ESA from the $^4F_{9/2}$ level. A complex spectrum between 25 800 and 26 400 cm^{-1} is obtained when monitoring the $^4G_{9/2} \rightarrow {}^4I_{13/2}$ transition [Fig. 8(a), (2)]. This spectrum is largely unchanged when the red beam is blocked except for the line at 25 983 cm^{-1}. This peak is attributed to the $^4I_{11/2} \rightarrow {}^4G_{9/2}$ transition. Under this assumption the energy of the $^4G_{9/2}(1)$ sublevel is found to lie at 36 143 cm^{-1} in reasonable agreement with the value found for ESA in the $^4G_{9/2}$ level. Decay curves obtained in these two excitation schemes are also similar.

All other lines correspond to absorptions from the

TABLE III. Energies (cm^{-1}) of the $^4D_{5/2}$, $^4G_{9/2}$, and $^4G_{11/2}$ sublevels.

Label	$^4G_{9/2}$	$^4D_{5/2}$	$^4G_{11/2}$
a	36 162.6	37 936	26 026.3
b	36 168.0	38 014.8	26 033.4
c	36 332.8	38 253.8	26 269.4
d	36 370.7		26 276.6
e			26 322.9
f			26 341.1

ground state to the $^4G_{11/2}$ level. This is clearly shown by the identical excitation spectra obtained by monitoring the $^4G_{9/2} \rightarrow {}^4I_{13/2}$ or the $^4G_{11/2} \rightarrow {}^4I_{15/2}$ transitions [Fig. 8(a)]. This also suggests that up-conversion under excitation in the $^4G_{11/2}$ level is not due to energy transfer in doubly excited pairs but to an ESA process. This explanation has also been suggested for the same excitation in $CsMgCl_3:Er^{3+}$.[19] Another possibility to account for these results is to consider an overlap between $^4I_{15/2} \rightarrow {}^4G_{11/2}$ absorptions of ions in nonsymmetric dimers so that these complexes could also be doubly excited. From the most intense lines of these spectra we determined the energies of the $^4G_{11/2}$ sublevels of Er^{3+} in symmetric pairs, taking into account the second sublevel of the fundamental multiplet at 30 cm^{-1} because its population cannot be neglected at the sample temperature (Table III).

Excitation lines observed only under double pumping between 25 550 and 25 700 cm^{-1} [Fig. 8(b)] have a structure very close to the one obtained in the ESA experiment for the $^4D_{5/2}$ level. For example, relative energy positions of the lines differ only by 1 or 2 cm^{-1} between the two experiments. From these results, it seems very unlikely that these lines could correspond to transitions from the $^4F_{9/2}$ level. We rather suggest that these lines originate from the $^4I_{9/2} \rightarrow {}^4D_{5/2}$ transition. In this case the energies of the first three components of the $^4D_{5/2}$ level are in excellent agreement with those found for ESA in the $^4D_{5/2}$ level (difference smaller than 2 cm^{-1}).

In this experiment, we were not able to record a transition to the $^2I_{11/2}$ level. This is perhaps explained by the proximity between the energy of this level [estimated at 40 800 cm^{-1} (Ref. 19)] and the absorption of the host (40 000 cm^{-1}) (Refs. 25 and 26).

IV. ANTI-STOKES FLUORESCENCE DYNAMICS

A. Introduction

Time-resolved anti-Stokes emissions of the $^4G_{9/2}$ and $^4G_{11/2}$ levels have been recorded using different up-conversion processes: excited-state absorption to reach the $^4D_{5/2}$ and $^4G_{9/2}$ levels or energy transfer in doubly excited pairs in the $^4S_{3/2}$, $^4F_{7/2}$, and $^4F_{5/2}$ levels. In some cases, the decay of the $^4D_{5/2}$ level was also measured.

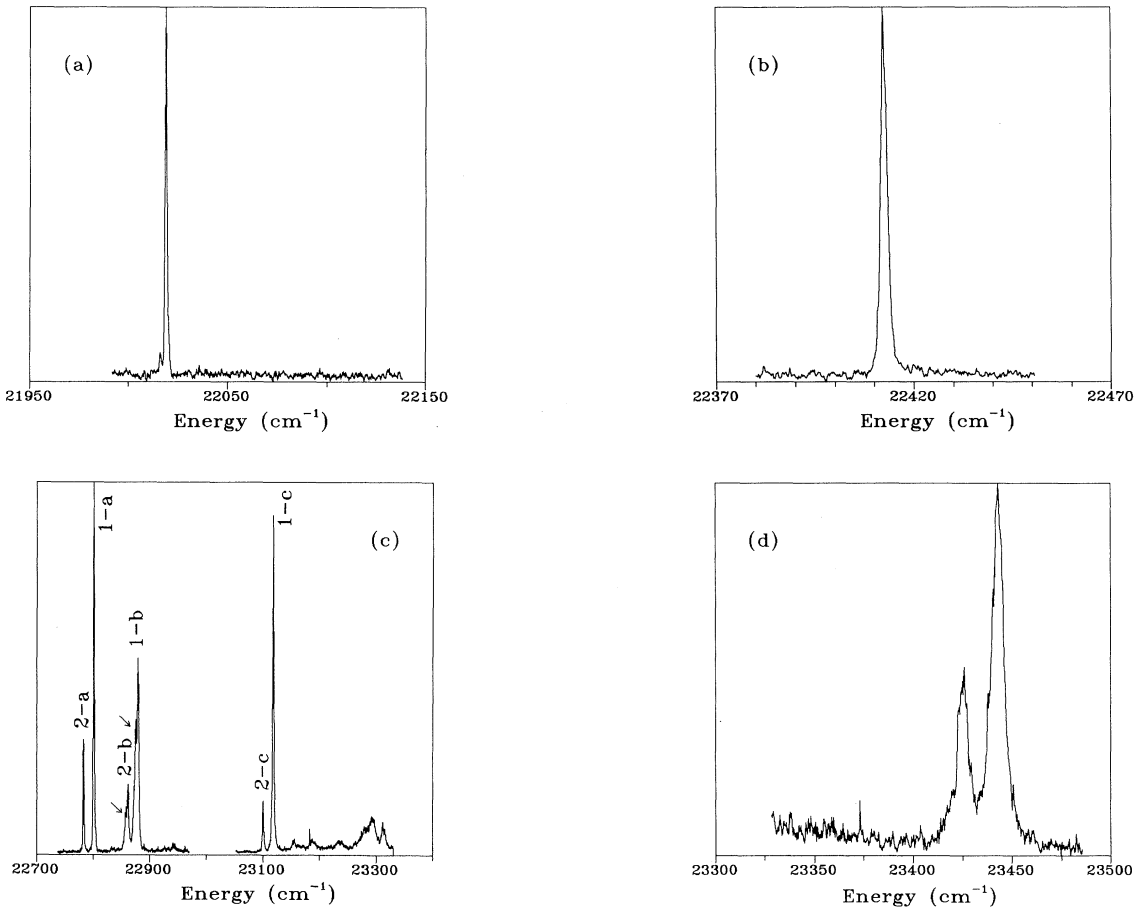

FIG. 7. (a) $^4I_{15/2} \rightarrow {}^4F_{5/2}$, (b) $^4I_{15/2} \rightarrow {}^4F_{3/2}$ (c) $^4F_{9/2} \rightarrow {}^4D_{5/2}$, and (d) $^4F_{9/2} \rightarrow {}^4D_{7/2}$ excitation spectra monitoring $^4G_{9/2} \rightarrow {}^4I_{13/2}$ emission. (Transition labels refer to Table III.)

As shown, for example, in Figs. 11(a), 13(a), 15(a), and 17(b) for the $^4G_{9/2}$ level, each excitation results in a particular fluorescence dynamic, often complex and not explained by usual multiphonon relaxation schemes. In general, mechanisms proposed to explain and fit these experimental curves are based on cross relaxation inside a Er^{3+} pair which is the dominant center in this material (see the Introduction). This implies that pair states and not ion levels have to be considered in the treatment of the fluorescence dynamics, even if the levels are not energetically affected by pair effects. As a matter of fact, splitting of rare-earth ions due to pair interaction scarcely exceeds a few tenths of cm^{-1}.[2,10] If i and j designate two levels of the ion, the decay rate $w(i,j)$ of the pair state (i,j) is obtained by the relation

$$w(i,j)=\Omega_i+\Omega_j+w_T(i,j)\ ,$$

where Ω_i and Ω_j are the ions' relaxation rates and $w_T(i,j)$ the total probability of transfer between the ions in i and j states.

Difficulties sometimes arise in decay measurements because emission from a level can be due to several pair states of different lifetimes. Complexity of this problem increases when the energy difference between the excited and analyzed levels is large. Moreover, precise determination of $w_T(i,j)$ when i and j are excited levels is only possible when $w_T(i,g)$ and $w_T(j,g)$ (g designates the ground state) are negligible compared to w_i, w_j, and $w_T(i,j)$. Doubly excited states (i,i) can also modify the value of $w(i,g)$ when the excitation power density is high. To take into account strong energy transfer, w_i can be accessed by measuring samples codoped with trivalent and monovalent ions. In this case M^{3+}-M^{+} dimers are formed in which the trivalent ion is in a site close to that of ions in M^{3+}-vacancy-M^{3+} complexes. Energy transfer is, however, not possible in mixed dimers. In opposition, isolated ions in single-doped compounds do not provide reliable values because of their low concentration and their crystallographic sites which differ from pair ones.

When the final state is known (from energy conservation, for example), analysis of the processes which produce it must often include several simultaneous mechanisms with various numbers of intermediate states.[20] This is especially true for Er^{3+} ions which have a large number of levels under 40 000 cm^{-1}.

Most of the proposed mechanisms in our interpretation include only one intermediate level between initial and final states. Figure 9(a) illustrates the following mecha-

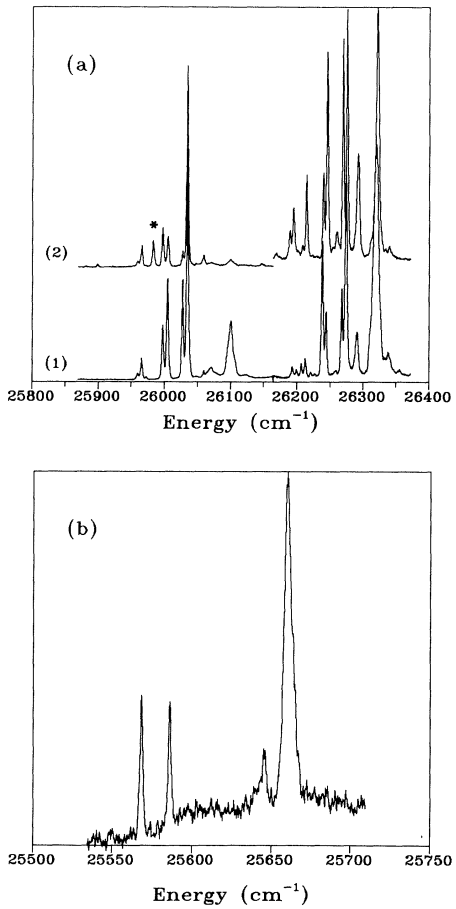

FIG. 8. (a) $^4I_{15/2}\rightarrow{}^4G_{11/2}$ excitation spectra monitoring (1) $^4G_{11/2}\rightarrow{}^4I_{15/2}$ and (2) $^4G_{9/2}\rightarrow{}^4I_{13/2}$ emissions. (* corresponds to $^4I_{11/2}\rightarrow{}^4G_{9/2}$ transition.) (b) $^4I_{9/2}\rightarrow{}^4D_{5/2}$ excitation spectrum monitoring $^4G_{9/2}\rightarrow{}^4I_{13/2}$ emission.

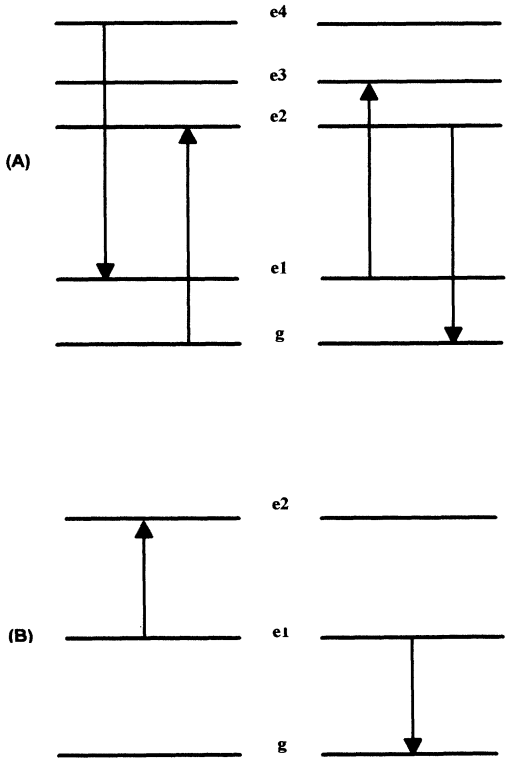

FIG. 9. (a) Successive cross-relaxation processes in a pair. (b) Up-conversion by energy transfer in a doubly excited dimer.

nism:

$$(e4,g)\rightarrow(e2,e1)\rightarrow(e3,g)\ . \qquad \text{(M1)}$$

Population of the $(e4,g)$, $(e2,e1)$, and $(e3,g)$ pair states is described by the following equations where $N_4=N(e4,g)$, $N_3=N(e2,e1)$, $N_2=N(e3,g)$:

$$\frac{dN_4}{dt}=-w_4N_4\ , \qquad (1)$$

$$\frac{dN_3}{dt}=-w_3N_3+\phi_{43}w_4N_4\ , \qquad (2)$$

$$\frac{dN_2}{dt}=-w_2N_2+\phi_{32}w_3N_3\ , \qquad (3)$$

w_i is the relaxation rate of pair i and ϕ_{ij} the branching ratio from i to j. The solutions of these equations are

$$N_4=N_4^0\exp(-w_4t)\ , \qquad (4)$$

$$N_3=\frac{\phi_{43}w_4N_4^0}{w_4-w_3}[\exp(-w_4t)-\exp(-w_3t)]\ , \qquad (5)$$

$$N_2=\frac{\phi_{43}w_4\phi_{32}w_3N_4^0}{(w_4-w_2)(w_3-w_4)(w_3-w_2)}\times[(w_2-w_3)\exp(-w_4t)+(w_4-w_2)\exp(-w_3t)+(w_3-w_4)\exp(-w_2t)]\ . \qquad (6)$$

N_4^0 is the initial population of the pair state number 4.

A second process which can compete with (M1) is the multiphonon relaxation from the $(e4,g)$ state to the $(e3,g)$ state [process (M2)]. Equation (3) then becomes

$$\frac{dN_2}{dt}=-w_2N_2+\phi_{32}w_3N_3+\phi_{42}w_4N_4 \qquad (7)$$

and the new solution is

$$N_2=\frac{\phi_{43}w_4\phi_{32}w_3N_4^0}{(w_4-w_2)(w_3-w_4)(w_3-w_2)}[(w_2-w_3)\exp(-w_4t)+(w_4-w_2)\exp(-w_3t)+(w_3-w_4)\exp(-w_2t)]+\frac{\phi_{42}w_4N_4^0}{w_2-w_4}[\exp(-w_4t)-\exp(-w_2t)]\ . \qquad (8)$$

A typical temporal variation for N_2 is presented in Fig. 10.

In this case, it is important to estimate the parameters which determine the relative intensities of these two processes for the population of the final state 2. These intensities can be evaluated by the integral

$$I_N=\int_0^\infty N(t)dt\ .$$

For levels 2, 3, and 4, this calculation gives the following results:

$$I_4=\frac{N_4^0}{w_4}\ ,$$

$$I_3=\frac{\phi_{43}N_4^0}{w_3}\ ,$$

$$I_2=\frac{N_4^0}{w_2}(\phi_{43}\phi_{32}+\phi_{42})\ .$$

The relative intensities of the (M1) and (M2) processes in the I_2 integral depend directly only on the ϕ_{ij} branching ratios and not on the relative values of the different transfer rates $\phi_{ij}w_i$. Two processes can compete only if they satisfy the condition $\phi_{43}\phi_{32}\sim\phi_{42}$. This implies $\phi_{43}>\phi_{42}$ [condition C1)] and $\phi_{32}>\phi_{42}$ [condition (C2)] since all branching ratios are lower than one. Only the first of these two necessary conditions can be simply evaluated by comparing the energy mismatches of the processes starting from level 4. In our example, (M1) can compete with (M2) only if the relaxation probability from level 4 to level 3 ($\phi_{43}w_4$) is larger than that of level 4 to level 2 ($\phi_{42}w_4$). However, the relative values of the branching ratios $\phi_{42}w_4$ and $\phi_{32}w_3$ are not necessarily conclusive on the condition $\phi_{32}>\phi_{42}$, especially in the case $w_4\gg w_3$. So, it is possible to observe a competition between (M1) and (M2) even if the $3\rightarrow2$ relaxation is less resonant than the $4\rightarrow2$ one.

The extension of this calculation to a process (Q1) which involves n intermediate levels competing with a second one (Q2) with m intermediate levels (with $m<n$) gives the following results (i and j subscripts, respectively, correspond to the final and initial states and ϕ_i to the

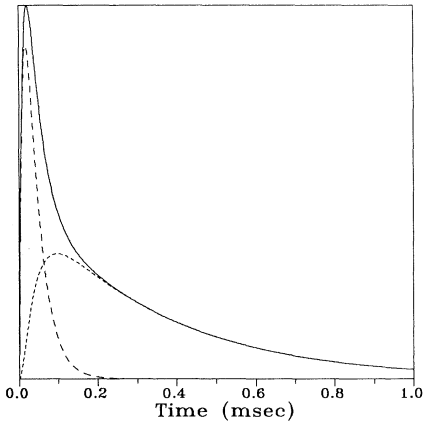

FIG. 10. Population of the final state computed with Eq. (8) in the three-level model incuding competition between direct (dashed curve) and indirect (dotted line) relaxations. ($w_4=100\,000$ sec^{-1}, $w_3=3000$ sec^{-1}, $w_2=30\,000$ sec^{-1}, and $\phi_{43}\phi_{32}\phi_{42}^{-1}=2.91$.)

different branching ratios):

$$I_f^{Q1}=\frac{N_i^0}{w_f}\prod_1^n \phi_k \ ,$$

$$I_f^{Q2}=\frac{N_i^0}{w_f}\prod_1^m \phi_l'$$

with $I_f=I_f^{Q1}+I_f^{Q2}$. In order that $I_f^{Q1}\approx I_f^{Q2}$ the following condition has to be satisfied:

$$\forall k \ , \ \phi_k > \prod_1^n \phi_l' \ .$$

It is therefore difficult to appreciate in the general case the possibility of a competition by considering only the energy mismatches, except for very nonresonant mechanisms leading to $\phi_i \sim 0$.

Most of the mechanisms proposed in the discussion will include the more resonant direct relaxations competing with processes involving an intermediate level and satisfying the (C1) condition. For more complex processes, relaxations have been determined by comparing the results of the different excitations and excluding poorly resonant transfers since branching ratios between pair states are difficult to measure. All energy mismatches for the proposed relaxations in our interpretation are listed in Table IV.

In order to establish the rate equations of the different pair states which are implied in a mechanism, a simplification has been made to use the preceding systems of equations. We considered that the final states which share a common level have a similar lifetime. As a matter of fact, experimental decays are well described using this assumption.

B. Discussion

1. General results on ESA

Fluorescence decays of the $^4D_{5/2}$ and $^4G_{9/2}$ levels directly excited by ESA exhibit a single exponential behavior without any rise time. This confirms the assignment of the emissions from these levels. The decay times of the corresponding pair states are the following:

$$\tau[(^4D_{5/2}\ ,^4I_{15/2})]=1.5\ \mu\text{sec} \ ,$$

$$\tau[(^4G_{9/2}\ ,^4I_{15/2})]=35.3\ \mu\text{sec} \ .$$

The second value is in agreement with Ref. 17.

Concerning the different types of pairs, ESA does not have the selectivity of the up-conversion in doubly excited dimers (Sec. III A). Hence, measured values of pair state decay times can differ from those recorded in one exciting beam experiment.

2. Absorption in the $^4F_{9/2}$ excited states to the $^4G_{9/2}$ level

The $^4G_{11/2}$ level transient, analyzed by Eq. (5), exhibits a 6-μsec rise time and a 32.4-μsec decay time. This suggests a direct population of this level from the $^4G_{9/2}$ level which can be explained by the cross relaxation:

$$(^4G_{9/2}\ ,^4I_{15/2})\rightarrow(^4G_{11/2}\ ,^4I_{11/2}) \ . \qquad \text{(P1)}$$

In this case, the decay measured for the $^4G_{11/2}$ level when excited in the $^4G_{9/2}$ level corresponds to the $(^4G_{11/2},^4I_{11/2})$ pair state (which has therefore a 6-μsec lifetime). This first result already reflects the special nature of pair dynamic analysis evoked in Sec. IV A.

TABLE IV. Energy mismatches of relaxations involved in the proposed processes for fluorescence dynamics. Values smaller than 30 cm^{-1} are not indicated for the corresponding transfers which are considered to be resonant.

Pair relaxation	Process
$(^4D_{5/2},^4I_{15/2})\rightarrow(^4F_{9/2},^4F_{3/2})+227\ cm^{-1}\rightarrow(^4F_{9/2},^4F_{5/2})$	(P2)
$(^4D_{5/2},^4I_{15/2})\rightarrow(^2H_{11/2},^4S_{3/2})+539\ cm^{-1}\rightarrow(^4S_{3/2},^4S_{3/2})$	
$(^4D_{5/2},^4I_{15/2})\rightarrow(^2H_{9/2},^4I_{9/2})+1045\ cm^{-1}$	
$(^4G_{9/2},^4I_{15/2})\rightarrow(^4G_{11/2},^4I_{11/2})$	(P1)
$(^2P_{3/2},^4I_{9/2})\rightarrow(^2G_{7/2},^4I_{9/2})+3650\ cm^{-1}\rightarrow(^4G_{11/2},^4I_{9/2})$	(P7)
$(^2H_{9/2},^4S_{3/2})\rightarrow(^4G_{9/2},^4I_{13/2})$	(P9)
$(^2H_{9/2},^4I_{9/2})\rightarrow(^4G_{9/2},^4I_{15/2})+122\ cm^{-1}$	(P3)
$(^4F_{5/2},^4F_{5/2})\rightarrow(^2P_{3/2},^4I_{9/2})$	(P7)
$(^4F_{5/2},^4F_{5/2})\rightarrow(^4G_{9/2},^4I_{13/2})+1000\ cm^{-1}$	(P8)
$(^4F_{5/2},^4F_{5/2})\rightarrow(^2H_{9/2},^2H_{11/2})+481\ cm^{-1}\rightarrow(^2H_{9/2},^4S_{3/2})$	(P9)
$(^4F_{5/2},^4F_{5/2})\rightarrow(^2G_{7/2},^4F_{9/2})+731\ cm^{-1}\rightarrow(^4G_{11/2},^4F_{9/2})$	(P6)
$(^4F_{5/2},^4S_{3/2})\rightarrow(^2G_{7/2},^4I_{9/2})\rightarrow(^4G_{11/2},^4I_{9/2})$	(P12)
$(^4F_{5/2},^4F_{9/2})\rightarrow(^4G_{9/2},^4I_{15/2})+523\ cm^{-1}$	(P2a)
$(^4F_{5/2},^4F_{9/2})\rightarrow(^2H_{9/2},^4I_{9/2})+258\ cm^{-1}$	(P3a)
$(^4F_{7/2},^4F_{7/2})\rightarrow(^4D_{5/2},^4I_{15/2})+2100\ cm^{-1}$	(P10)
$(^4F_{7/2},^4F_{7/2})\rightarrow(^4S_{3/2},^4S_{3/2})+2400\ cm^{-1}$	(P11)
$(^4F_{7/2},^4F_{7/2})\rightarrow(^4F_{5/2},^4S_{3/2})$	(P12)
$(^4S_{3/2},^4S_{3/2})\rightarrow(^4G_{9/2},^4I_{15/2})$	(P4) (P11)
$(^4S_{3/2},^4S_{3/2})\rightarrow(^4G_{11/2},^4I_{11/2})+239\ cm^{-1}$	(P5)

3. *Absorption in the $^4F_{9/2}$ excited state to the $^4D_{5/2}$ level*

(a) Decay of the $^4G_{9/2}$ level. The time dependence of the $^4G_{9/2}$ level emission clearly shows that a simple multiphonon relaxation from the $^4D_{5/2}$ level cannot explain the experimental curve [Fig. 11(a)]. The long part of the transient, with a decay rate of about 250 μsec, does not correspond to the $(^4G_{9/2},^4I_{15/2})$ pair state lifetime (35.3 μsec) and the rise process exhibits no short component in agreement with the lifetime of the $(^4D_{5/2},^4I_{15/2})$ state (1.5 μsec). This can be explained by assuming that the intrapair cross-relaxation mechanisms dominate the $^4D_{5/2}\rightarrow{}^4G_{9/2}$ multiphonon relaxation. Several cross relaxations involving small energy mismatches can occur from the $(^4D_{5/2},^4I_{15/2})$ state. Some of the pair states resulting from these cross relaxations can relax very quickly since weakly separated levels have a short lifetime. In the following, we will not take into account such short-lived states. However, they can be found in Table IV.

The triply excited pair states such as $(^4D_{5/2},^4F_{9/2})$ are also neglected in our models, since the low power of the continuous beam allows one to avoid up-conversion without pulsed excitation which arises in doubly excited dimers at 659.9 nm.[12]

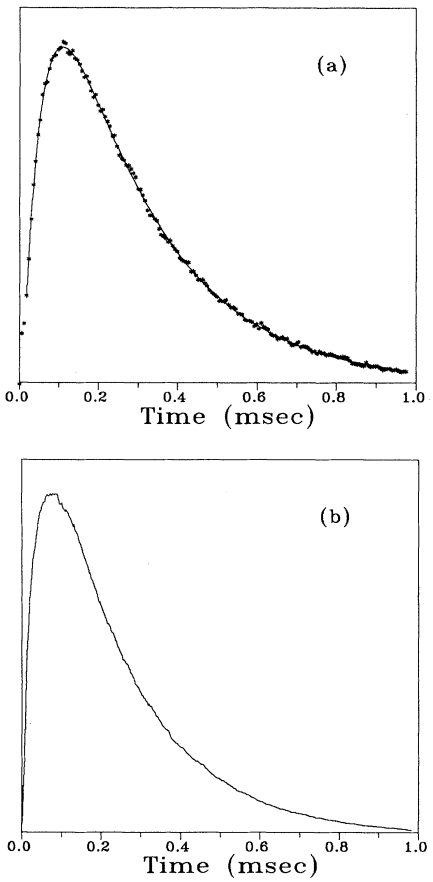

FIG. 11. (a) $^4G_{9/2}\rightarrow{}^4I_{13/2}$ and (b) $^4G_{11/2}\rightarrow{}^4I_{15/2}$ fluorescence transients after excitation in the $^4D_{5/2}$ level by ESA (stars, experimental result; solid curve, calculated curve).

Starting from these pair states a second cross relaxation can populate the $^4G_{9/2}$ level through the $(^4G_{9/2},^4I_{15/2})$ pair state. A pair state including the $^4G_{9/2}$ level with another excited level cannot be obtained since the energy difference between $^4D_{5/2}$ and $^4G_{9/2}$ levels is too small. The possible transitions to $(^4G_{9/2},^4I_{15/2})$ are

$$(^4F_{5/2},^4F_{9/2})\rightarrow(^4G_{9/2},^4I_{15/2}),$$

$$(^4S_{3/2},^4S_{3/2})\rightarrow(^4G_{9/2},^4I_{15/2}),$$

$$(^2H_{9/2},^4I_{9/2})\rightarrow(^4G_{9/2},^4I_{15/2}).$$

The relaxation from $(^4G_{11/2},^4I_{11/2})$ is not considered here because we showed that upon direct excitation in the $^4G_{9/2}$ level, (P1) is the main process since no sign of back transfer has been found.

From the $(^4D_{5/2},^4I_{15/2})$ pair state, two routes dissipating less than 600 cm^{-1} for each relaxation step can be proposed to populate $(^4G_{9/2},^4I_{15/2})$ through one intermediate state:

$$(^4D_{5/2},^4I_{15/2})\rightarrow(^4F_{5/2},^4F_{9/2})\rightarrow(^4G_{9/2},^4I_{15/2}), \quad \text{(P2)}$$

$$(^4D_{5/2},^4I_{15/2})\rightarrow(^4S_{3/2},^4S_{3/2})\rightarrow(^4G_{9/2},^4I_{15/2}).$$

As explained before (Sec. IV A) in the case of processes involving several intermediate states, comparison between energy mismatches (Table IV) gives no definite indication about the most probable process. On the other hand, study of up-converted emissions resulting from excitation in the $^4S_{3/2}$ level (Sec. IV B 5) shows that the $(^4S_{3/2},^4S_{3/2})$ pair state has a lifetime of 11 μsec. This value is not in agreement with the long rise process as shown on the experimental curve [Fig. 11(a)]. The main process to be considered is then (P2) (Fig. 12).

This process, well described by Eq. (5) since $\tau(^4D_{5/2},^4I_{15/2})$ is negligible, does not, however, give a good approximation of the experimental data because it cannot describe both rise and decay times, which are longer than the $(^4G_{9/2},^4I_{15/2})$ pair state lifetime. The only possible intermediate state $(^2H_{9/2},^4I_{9/2})$ is proposed to take into account this discrepancy following this scheme (Fig. 12):

$$(^4D_{5/2},^4I_{15/2})\rightarrow(^4F_{5/2},^4F_{9/2})\rightarrow(^2H_{9/2},^4I_{9/2})\rightarrow(^4G_{9/2},^4I_{15/2}). \quad \text{(P3)}$$

The $(^4S_{3/2},^4S_{3/2})$ pair state is again not considered due to its short lifetime.

The competition between (P2) and (P3) satisfies the (C1) condition concerning the resonance since the (P2a) relaxation dissipates less phonons than the (P3a) process (Table IV).

The resulting populations after addition of (P2) and (P3) are described by Eqs. (1), (2), and (7) in which the 4, 3, and 2 levels represent, respectively, the $(^4F_{9/2},^4F_{5/2})$, $(^2H_{9/2},^4I_{9/2})$, and $(^4G_{9/2},^4I_{15/2})$ states.

A least-squares fit of the experimental curve has been performed using Eq. (8) and the calculated curve is

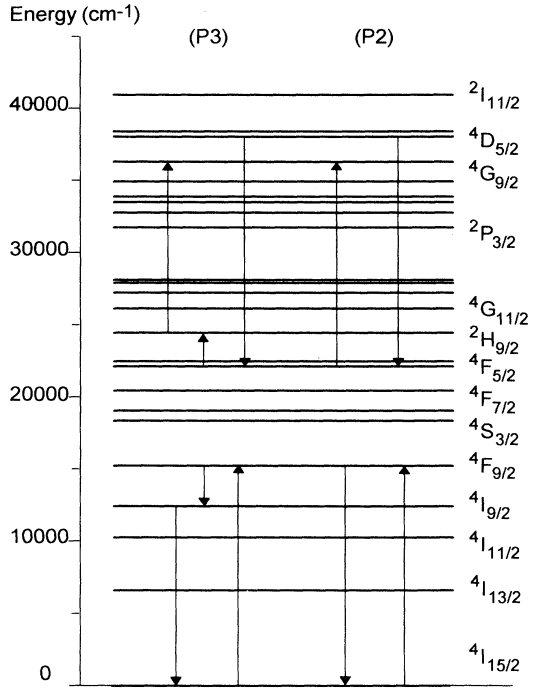

FIG. 12. (P2) and (P3) pair relaxation processes.

presented in Fig. 11(a). The following parameters have been determined using for w_2 the numerical value of the $(^4G_{9/2},^4I_{15/2})$ pair state lifetime measured in the ESA experiment (Sec. IV B 2):

$$w_4=w(^4F_{9/2},^4F_{5/2})=18\,545\ \text{sec}^{-1}\ ,$$

$$w_3=w(^2H_{9/2}\ ,^4I_{9/2})=4140\ \text{sec}^{-1}\ ,$$

$$\phi_{43}\phi_{32}\phi_{42}^{-1}=6.51\ .$$

(b) Decay of the $^4G_{11/2}$ level. The $^4G_{11/2}$ transient is rather similar to the $(^4G_{9/2},^4I_{15/2})$ pair state one as shown in Figs. 11(a) and 11(b), especially in their long part. This can be interpreted by considering that the $^4G_{11/2}$ level is mainly populated from the $(^4G_{9/2},^4I_{15/2})$ state by the (P1) process and by neglecting the $(^4G_{11/2},^4I_{11/2})$ pair lifetime of 6 μsec (Sec. IV B 2).

4. General results on up-conversion in doubly excited dimers

The case of up-conversion in doubly excited pairs can be treated as the one previously described, i.e., cross relaxation between coupled ions. Equations (1) and (2) can be applied to this kind of process in which levels 4 and 3 stand for $(e1,e1)$ and $(e2,g)$ states [Fig. 9(b)]. The measure of the decay time of the highest anti-Stokes emission allows one to determine the w_4 decay rate of the doubly excited pair providing that w_3 is known, for example, from direct excitation in the $(e2,g)$ pair state. The transfer rate w_T for up-conversion can then be estimated from w_4 by the relation $w_T=w_4-2w(e1,g)$ because w_4 is usually much larger than $w(e1,g)$. The value of w_T obtained in this way is anyhow a minimum.

Under excitation in the $^4S_{3/2}$ level, good agreement is observed between experimental and fitted curves (Fig. 13) computed with Eq. (5). This confirms that neither transfer between pairs nor the ESA process, which could lead to anti-Stokes emission, occur. The excitation and emission spectra recorded when exciting in the $^4F_{7/2}$ level (Sec. III A) also show that Er^{3+} isolated ions or substituted in nonsymmetric dimers cannot give rise to up-converted emissions. The same conclusion is valid for the other excitations since up-converted emission spectra are strictly similar in all cases. This is in agreement with previously reported results.[17,18]

5. Up-conversion with excitation in the $^4S_{3/2}$ level

Decay of $^4G_{9/2}$ and $^4G_{11/2}$ levels. Under this excitation, according to the energy of the involved levels, $^4G_{9/2}$ and $^4G_{11/2}$ can be directly populated to give the following pair states (see Fig. 14):

$$(^4S_{3/2},^4S_{3/2})\rightarrow(^4G_{9/2},^4I_{15/2})\ , \qquad \text{(P4)}$$

$$(^4S_{3/2},^4S_{3/2})\rightarrow(^4G_{11/2},^4I_{11/2})\ . \qquad \text{(P5)}$$

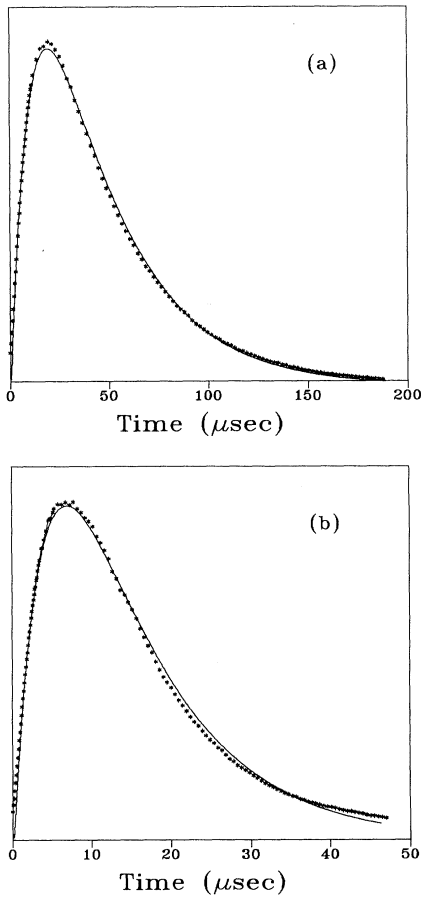

FIG. 13. (a) $^4G_{9/2}\rightarrow{}^4I_{13/2}$ and (b) $^4G_{11/2}\rightarrow{}^4I_{15/2}$ fluorescence transients under excitation in the $^4S_{3/2}$ level (stars, experimental result; solid curve, calculated curve).

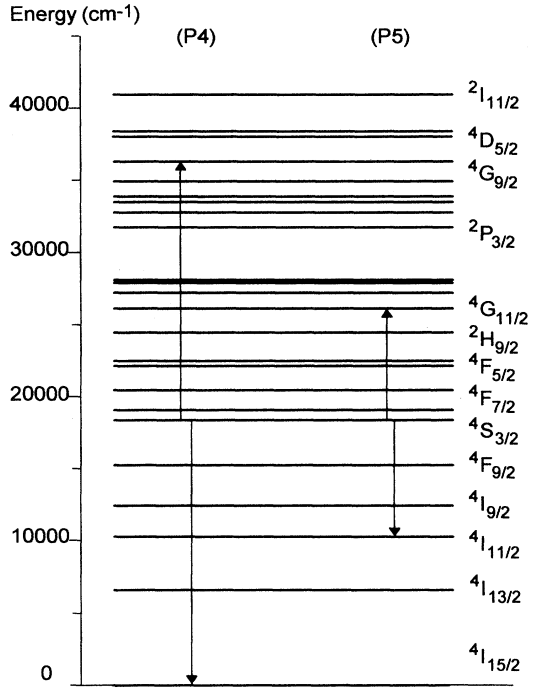

FIG. 14. (P4) and (P5) pair relaxation processes.

In these cases, the population of the excited level is described by Eq. (5). The experimental transients were fitted using this model with the following parameters [Figs. 13(a) and 13(b)]:

$$w(^4S_{3/2},{}^4S_{3/2})=89\,930\ \text{sec}^{-1}\ ,$$

$$w(^4G_{9/2},{}^4I_{15/2})=27\,624\ \text{sec}^{-1}\ ,$$

$$w(^4G_{11/2},{}^4I_{11/2})=225\,075\ \text{sec}^{-1}\ .$$

These values agree with the results obtained in the case of the $^4F_{9/2}$ excited-state absorption to the $^4G_{9/2}$ level. This interpretation is confirmed by the good match of the proposed transfers (Table IV). The transfer rate for up-conversion can be estimated from the $(^4S_{3/2},{}^4I_{15/2})$ pair state lifetime (410 μsec):

$$w_T\sim w(^4S_{3/2},{}^4S_{3/2})^{-1}-2w(^4S_{3/2},{}^4I_{15/2})$$
$$=8.5\times10^4\ \text{sec}^{-1}\ .$$

6. *Up-conversion with excitation in the $^4F_{5/2}$ level*

Decay of $^4G_{9/2}$ and $^4G_{11/2}$ levels. The time behavior of the anti-Stokes emission transients from the $^4G_{9/2}$ and $^4G_{11/2}$ levels [Figs. 15(a) and 15(b)] is very similar to the curve of Fig. 10 calculated by Eq. (8) which concerns a three-level system comprising two possibilities to populate the final state.

In the case of the $^4G_{11/2}$ level, the direct process which can populate this level in the most resonant way is the following:

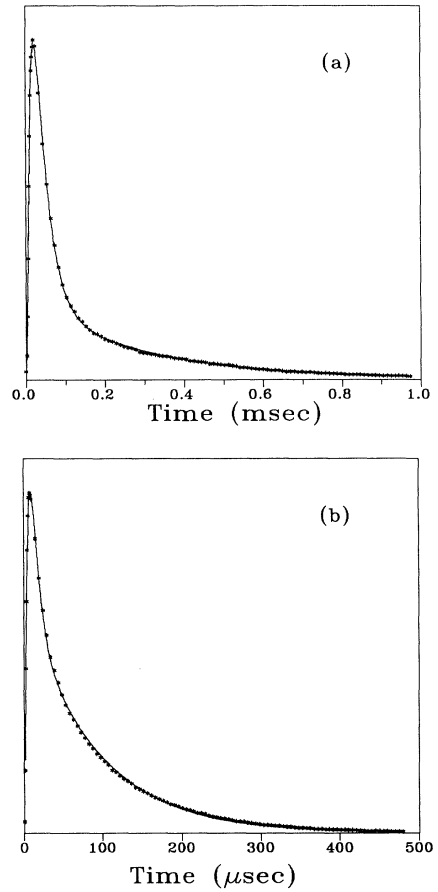

FIG. 15. (a) $^4G_{9/2}\rightarrow{}^4I_{13/2}$ and (b) $^4G_{11/2}\rightarrow{}^4I_{15/2}$ fluoresence transients under excitation in the $^4F_{5/2}$ level (stars, experimental result; solid curve, calculated curve).

$$(^4F_{5/2},{}^4F_{5/2})\rightarrow(^4G_{11/2}\ ,{}^4F_{9/2})\ . \qquad \text{(P6)}$$

In this model, we neglect the relaxation from $^2G_{7/2}$ to $^4G_{11/2}$.

The long part of the decay is ascribed to a process which involves an intermediate level, the (C1) initial condition for energy mismatch being satisfied as reported in Table IV:

$$(^4F_{5/2},{}^4F_{5/2})\rightarrow(^2P_{3/2},{}^4I_{9/2})\rightarrow(^4G_{11/2},{}^4I_{9/2})\ . \qquad \text{(P7)}$$

These mechanisms are schematized in Fig. 16.

Since the lifetime of the $^4I_{9/2}$ level has been found to be 10 msec,[18] we neglect relaxation from this level. Assuming that the lifetimes of the $(^4G_{11/2},{}^4F_{9/2})$ and $(^4G_{11/2},{}^4I_{9/2})$ pair states are very close, the addition of the (P6) and (P7) processes corresponds to Eqs. (4), (5), and (7) where levels 4, 3, and 2 represent, respectively, the $(^4F_{5/2},\ {}^4F_{5/2})$, $(^2P_{3/2},{}^4I_{9/2})$, and $(^4G_{11/2},{}^4I_{9/2}$ or $^4F_{9/2})$ pair states. The experimental curve has been fitted with Eq. (8) and the calculation gives the following numerical values:

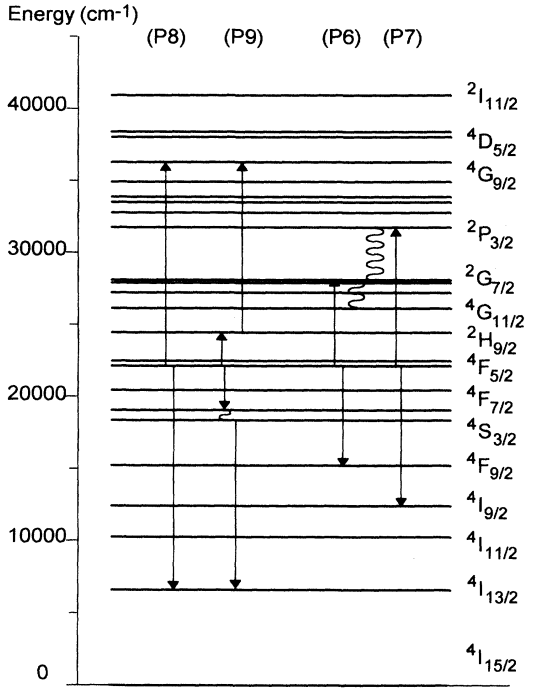

FIG. 16. (P6), (P7), (P8), and (P9) pair relaxation processes.

$$w(^4F_{5/2},{}^4F_{5/2}) = 122\,610 \text{ sec}^{-1} ,$$

$$w(^2P_{3/2},{}^4I_{9/2}) = 11\,415 \text{ sec}^{-1} ,$$

$$\phi_{43}\phi_{32}\phi_{42}^{-1} = 3.81 .$$

We used for $w(^4G_{11/2},{}^4I_{9/2}$ or $^4F_{9/2})$ the value obtained in the up-conversion experiment with excitation in the $^4S_{3/2}$ level.

Theoretical and experimental curves are shown in Fig. 15(b). The lifetime of the $(^2P_{3/2},{}^4I_{9/2})$ state is close to the one we measured for the $(^2P_{3/2},{}^4I_{15/2})$ pair state (100 μsec). The $^4I_{9/2}$ lifetime being long, this suggests that no cross relaxations occur in these states. Besides, even if relaxation from $^2P_{3/2}$ to $^2G_{7/2}$ dissipates 3600 cm^{-1}, the (C2) condition is not necessarily unsatisfied.

The transient of emission arising from the $^4G_{9/2}$ level [Fig. 15(a)] exhibits the same behavior as that of the $^4G_{11/2}$ level, so the same kind of mechanism is proposed. It involves direct and indirect relaxations. According to the energy of the initial pair state, a new state comprising the $^4G_{9/2}$ level can be obtained: $(^4G_{9/2},{}^4I_{13/2})$. We proposed the following routes to explain the experimental results:

$$(^4F_{5/2},{}^4F_{5/2}) \rightarrow (^4G_{9/2},{}^4I_{13/2}) , \quad \text{(P8)}$$

$$(^4F_{5/2},{}^4F_{5/2}) \rightarrow (^2H_{9/2},{}^4S_{3/2}) \rightarrow (^4G_{9/2},{}^4I_{13/2}) . \quad \text{(P9)}$$

The (P8) and (P9) processes (Fig. 16) seem to be the only ones able to populate directly, or through an intermediate state, the $^4G_{9/2}$ level. Another possibility would be to consider a transfer from the $(^4F_{5/2},{}^4F_{5/2})$ pair state to higher-energy levels and then fast relaxations to the $^4G_{9/2}$ state. This assumption is, however, not in agreement with the lack of emission of the $^4D_{5/2}$ level under

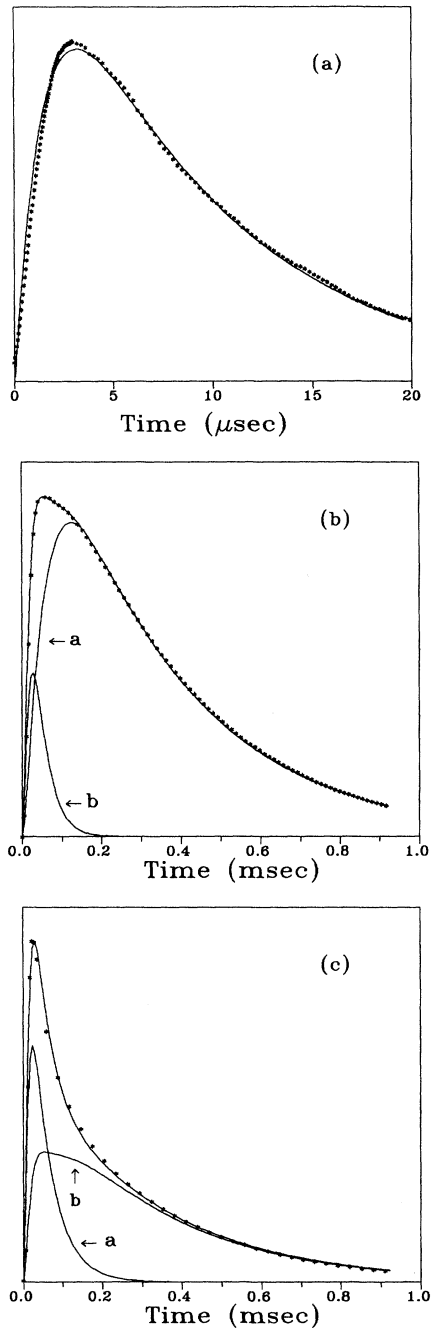

FIG. 17. (a) $^4D_{5/2} \rightarrow {}^4I_{13/2}$ fluorescence transients under excitation in the $^4F_{7/2}$ level (stars, experimental result; solid curve, calculated curve). (b) $^4G_{9/2} \rightarrow {}^4I_{13/2}$ fluorescence transients under excitation in the $^4F_{7/2}$ level [stars, experimental result; solid curve, calculated curve, (*a*) (P10) process, (*b*) (P11) process]. (c) $^4G_{11/2} \rightarrow {}^4I_{15/2}$ fluorescence transients under excitation in the $^4F_{7/2}$ level [stars, experimental result; solid curve, calculated curve, (*a*) (P12) process, (*b*) (P10′) process].

this excitation. Using the value calculated previously for the $(^4F_{5/2},^4F_{5/2})$ lifetime, fitting with Eq. (8) leads to the following decay rates:

$$w(^4G_{9/2},^4I_{13/2})=33\,671\ \text{sec}^{-1}\ ,$$

$$w(^2H_{9/2},^4S_{3/2})=3452.3\ \text{sec}^{-1}\ ,$$

$$\phi_{43}\phi_{32}\phi_{42}^{-1}=1.21\ .$$

The lifetimes of the $(^4G_{9/2},^4I_{13/2})$ and $(^2H_{9/2},^4S_{3/2})$ states are very close to the values found, respectively, for the $(^4G_{9/2},^4I_{15/2})$ and $(^2H_{9/2},^4I_{9/2})$ states in the ESA experiments. This result suggests that the cross-relaxation probability in these pairs is very close or smaller than multiphonon and radiative decay rates.

The transfer rate for up-conversion is estimated with the usual approximation since the $(^4F_{5/2},^4I_{15/2})$ lifetime is about 160 μsec:

$$w_T=w(^4F_{5/2},^4F_{5/2})-2w(^4F_{5/2},^4I_{15/2})$$
$$=1.1\times10^5\ \text{sec}^{-1}\ .$$

7. *Excitation in the $^4F_{7/2}$ level*

(a) Decay of the $^4D_{5/2}$ level. The decay of this level when excited in the $^4F_{7/2}$ level is reasonably approximated by Eq. (5) which involves only two levels. The three-level model [Eq. (6)] results in a very short lifetime for the additional state. The parameters of the fit by Eq. (5) are $(w_4)^{-1}=1.3$ μsec and $(w_3)^{-1}=7.73$ μsec [Fig. 17(a)]. The first lifetime is in good agreement with the decay time found in ESA experiments for the $(^4D_{5/2},^4I_{15/2})$ pair state. The second one, which is found as a rise time for all other emissions, is attributed to the $(^4F_{7/2},^4F_{7/2})$ pair state. Two mechanisms are possible: the $(^4F_{7/2},^4F_{7/2})$ pair can relax either directly to the $(^4D_{5/2},^4I_{15/2})$ state despite the large energy mismatch (2100 cm^{-1}) or to the $(^2I_{11/2},^4I_{15/2})$ state which would have then a very short lifetime. In this last case, the relaxation would be well resonant according to the position of the $^2I_{11/2}$ level in $CsMgCl_3$.[18] As explained in Sec. III B, no emission from the $^2I_{11/2}$ level was recorded to confirm this assumption.

However, for the treatment of the fluorescence transients, these two schemes are equivalent and we will consider that the $(^4F_{7/2},^4F_{7/2})$ state directly relaxes to the $(^4D_{5/2},^4I_{15/2})$ state. Given the lifetime of the $(^4F_{7/2},^4I_{15/2})$ state (210 μsec), the transfer rate for up-conversion is estimated to be 1.2×10^5 sec^{-1}.

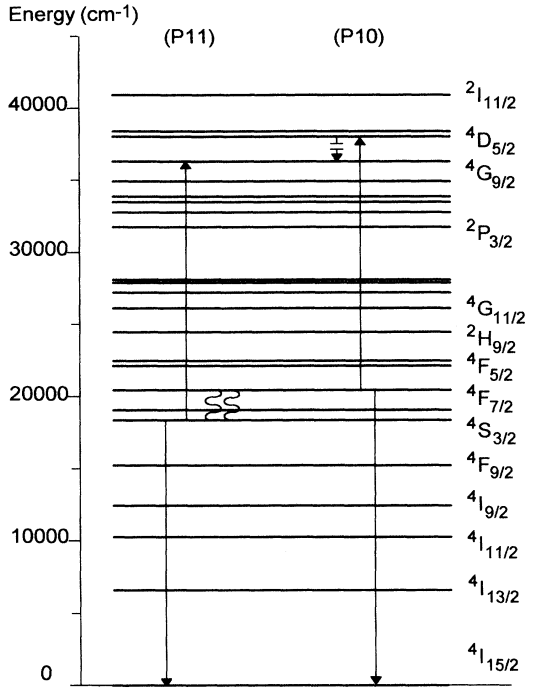

FIG. 18. (P10) and (P11) pair relaxation processes.

(b) Decay of the $^4G_{9/2}$ level. The up-converted fluorescence decay of this level is presented in Fig. 17(b). The curve is composed of two parts corresponding to long and fast mechanisms. The slow decaying part is similar to the transient recorded in ESA experiments where the $^4D_{5/2}$ level was directly excited. Introduction of the $(^4F_{7/2},^4F_{7/2})$ initial state, and of its relaxation to the $(^4D_{5/2},^4I_{15/2})$ state in the populating process of the $(^4G_{9/2}{}^4I_{15/2})$ state, described in Sec. IV B 3 (*a*), results in the following scheme (Fig. 18):

$$(^4F_{7/2},^4F_{7/2})\rightarrow(^4D_{5/2},^4I_{15/2})\rightarrow(^4F_{5/2},^4F_{9/2})\rightarrow(^2H_{9/2},^4I_{9/2})\rightarrow(^4G_{9/2},^4I_{15/2})$$
$$\rightarrow(^4G_{11/2},^4I_{15/2})\ . \qquad \text{(P10)}$$

Neglecting the lifetime of the $(^4D_{5/2},^4I_{15/2})$ state, corresponding populations are given by Eqs. (9)–(12) [and their solutions (13)–(16)] where the 5, 4, 3, and 2 levels, respectively, represent the $(^4F_{7/2},^4F_{7/2})$ $(^4F_{5/2},^4F_{9/2})$, $(^2H_{9/2},^4I_{9/2})$, and $(^4G_{9/2},^4I_{15/2})$ states:

$$\frac{dN_5}{dt}=-w_5N_5\ , \qquad (9)$$

$$\frac{dN_4}{dt}=-w_4N_4+\phi_1w_5N_5\ , \qquad (10)$$

$$\frac{dN_3}{dt}=-w_3N_3+\phi_2w_4N_4\ , \qquad (11)$$

$$\frac{dN_2}{dt} = -w_2 N_2 + \phi_3 w_3 N_3 + \phi_4 w_4 N_4 \ , \tag{12}$$

$$N_5 = N_5^0 \exp(-w_5 t) \ , \tag{13}$$

$$N_4 = \frac{\phi_1 w_5 N_5^0}{w_5 - w_4}[\exp(-w_4 t) - \exp(-w_5 t)] \ , \tag{14}$$

$$N_3 = \frac{\phi_2 w_4 \phi_1 w_5 N_5^0}{(w_4 - w_5)(w_5 - w_3)(w_4 - w_3)}[(w_3 - w_4)\exp(-w_5 t) + (w_5 - w_3)\exp(-w_4 t) + (w_4 - w_5)\exp(-w_3 t)] \ , \tag{15}$$

$$N_2 = \frac{\phi_3 w_3 \phi_2 w_4 \phi_1 w_5 N_5^0}{(w_4 - w_5)(w_5 - w_3)(w_4 - w_3)(w_5 - w_2)(w_4 - w_2)(w_3 - w_2)} \times [(w_4 - w_3)(w_4 - w_2)(w_3 - w_2)\exp(-w_5 t) + (w_5 - w_2)(w_3 - w_5)(w_3 - w_2)\exp(-w_4 t) + (w_5 - w_2)(w_4 - w_2)(w_5 - w_4)\exp(-w_3 t) + (w_5 - w_3)(w_5 - w_4)(w_3 - w_4)\exp(-w_2 t)] \ . \tag{16}$$

The parameter $w_3 = w(^2H_{9/2}, ^4I_{9/2})$ has been adjusted to fit the long component of the experimental decay. The difference between values of w_3 in ESA and this experiment is attributed to the influence of the nonsymmetric pairs (Sec. IV B 1). The calculated curve has then been subtracted from experimental values. The remaining decay corresponds to a fast process [Fig. 17(b)].

A new mechanism therefore populates the $(^4G_{9/2}, ^4I_{15/2})$ state which is the only one including the $^4G_{9/2}$ level that a two-photon process can reach starting from the $(^4F_{7/2}, ^4F_{7/2})$ state. From previous excitation results, $(^4S_{3/2}, ^4S_{3/2})$ is the only short-lived state able to relax to the $(^4G_{9/2}, ^4I_{15/2})$ state. The fast component obtained from the above subtraction was fitted using the values already known for the different pair states and the scheme (Fig. 18):

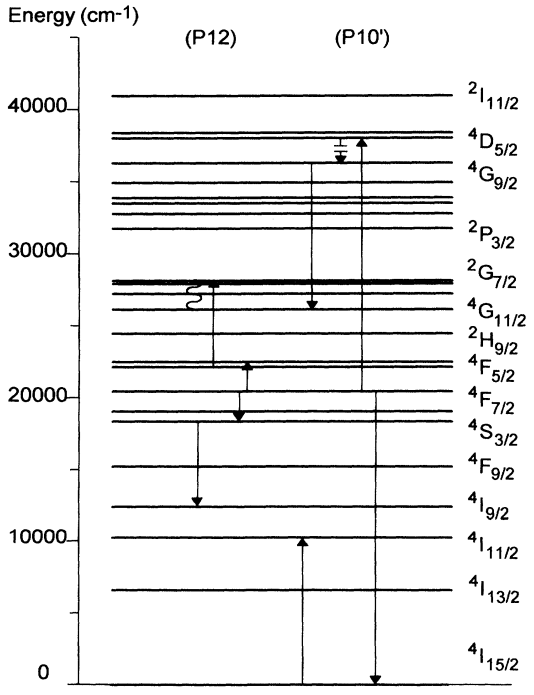

FIG. 19. (P10') and (P12) pair relaxation processes.

$$(^4F_{7/2}, ^4F_{7/2}) \rightarrow (^4S_{3/2}, ^4S_{3/2}) \rightarrow (^4G_{9/2}, ^4I_{15/2}) \ . \tag{P11}$$

Experimental and theoretical curves are shown in Fig. 17(b).

(c) Decay of the $^4G_{11/2}$ level. The study of this emission is as difficult as in the case of excitation in the $^4D_{5/2}$ level by ESA. However, as in this experiment, the long time part of the decay [Fig. 17(c)] corresponds to the $(^4G_{9/2}, ^4I_{15/2})$ transient state. We explain that by the $(^4G_{9/2}, ^4I_{15/2}) \rightarrow (^4G_{11/2}, ^4I_{11/2})$ cross relaxation following (P10) mechanism. In Fig. 19, this process is labeled (P10'). On the other hand, the short time part can be described by a three-level model in which the intermediate state has a lifetime of 50 μsec using for the $(^4F_{7/2}, ^4F_{7/2})$ and $(^4G_{11/2}, ^4I_{9/2})$ states the values previously determined. A possible mechanism is (Fig. 19)

$$(^4F_{7/2}, ^4F_{7/2}) \rightarrow (^4F_{5/2}, ^4S_{3/2}) \rightarrow (^4G_{11/2}, ^4I_{9/2}) \ . \tag{P12}$$

In this case, the lifetime of the $(^4F_{5/2}, ^4S_{3/2})$ state is close to that of the $(^4F_{5/2}, ^4F_{9/2})$ state. A rough approximation of the experimental curve is then possible by adding (P10) and (P11) processes and neglecting the lifetime of the final state $(^4G_{11/2}, ^4I_{11/2})$ [Fig. 17(c)].

V. CONCLUSION

$CsCdBr_3$ is a very appropriate host to study pair effects since trivalent ions enter nearly exclusively as charge-compensated complexes. Efficient UV and blue up-conversion has been observed under excitation in the $^4S_{3/2}$, $^4F_{7/2}$, and $^4F_{5/2}$ levels. Excitation in the $^4F_{7/2}$ level proved that up-conversion occurs only in symmetric M^{3+}-vacancy-M^{3+} dimers and not in nonsymmetric M^{3+}-M^{3+}-vacancy ones and can therefore be attributed to energy transfer between doubly excited ions in symmetric pairs. Seven emissions have been observed and ascribed to transitions from levels lying at high energy between 26 000 and 38 000 cm^{-1}.

To get more precise details on these levels, ESA experiments have been performed in the $^4F_{9/2}$ level to excite $^4D_{5/2}$ and $^4G_{9/2}$ states. Their lifetimes and multiplet energies were obtained in this way.

Fluorescence transients have been investigated for each excitation. $^4D_{5/2}$, $^4G_{11/2}$, and $^4G_{9/2}$ decays have been

fitted by models involving several competing cross relaxations. Up-conversion transfer rates have been estimated to be, respectively, 8.5×10^4, 1.2×10^5, and 1.1×10^5 sec^{-1}. These results show that this compound is an excellent candidate to study dynamics of complex intrapair processes.

ACKNOWLEDGMENTS

We wish to thank J. P. Denis, N. Gardant, and M. Genotelle for their help. Laboratoire de Physico-Chimie des Matériaux is Unité Propre du Centre National de la Recherche Scientifique No. 211.

[1]J. P. Jouart and G. Mary, Phys. Status Solidi B **149**, 633 (1988).

[2]J. C. Vial and R. Buisson, J. Phys. (Paris) **43**, L339 (1982).

[3]J. P. Jouart, C. Bissieux, and G. Mary, J. Lumin. **29**, 261 (1984).

[4]M. B. Seelbinder and J. C. Wright, J. Chem. Phys. **75**, 5070 (1981).

[5]R. Buisson, J. Q. Liu, and J. C. Vial, J. Phys. (Paris) **45**, 1533 (1984).

[6]A. Lezama, M. Oria, and C. B. de Araujo, Phys. Rev. B **33**, 4493 (1986).

[7]R. Buisson and J. C. Vial, J. Phys. (Paris) **42**, L115 (1981).

[8]F. Tong, W. P. Risk, R. M. Macfarlane, and W. Lenth, Electron. Lett. **25**, 1391 (1989).

[9]G. L. McPherson, J. A. Varga, and M. H. Nodine, Inorg. Chem. **18**, 2189 (1979).

[10]G. L. McPherson and L. M. Henling, Phys. Rev. B **16**, 1889 (1977).

[11]C. Barthou and R. B. Barthem, J. Lumin. **43**, 9 (1990).

[12]Ph. Goldner and F. Pellé, J. Lumin. **55**, 197 (1993).

[13]J. P. Chaminade, R. M. Macfarlane, F. Ramaz, and J. C. Vial, J. Lumin. **48 & 49**, 531 (1991).

[14]M. Mujaji, G. D. Jones, and R. W. G. Syme, J. Lumin. **53**, 473 (1992).

[15]A. Garavi and G. L. McPherson, Chem. Phys. Lett. **200**, 279 (1992).

[16]N. J. Cockroft, G. D. Jones, and R W. G. Syme, J. Lumin. **43**, 275 (1989).

[17]G. L. McPherson, A. Garavi, and S. L. Meyerson, Chem. Phys. **165**, 361 (1992).

[18]N. J. Cockroft, G. D. Jones, and D. C. N'Guyen, Phys. Rev. B **45**, 5187 (1992).

[19]G. L. McPherson and S. L. Meyerson, Chem. Phys. Lett. **179**, 325 (1991).

[20]D. R. Tallant, M. P. Miller, and J. C. Wright, J. Chem. Phys. **65**, 510 (1976).

[21]W. T. Carnall, P. R. Fields, and K. Rajnak, J. Chem. Phys. **49**, 4424 (1968).

[22]S. Buddhudu and F. J. Bryant, J. Less-Common Met. **147**, 213 (1989).

[23]G. H. Dieke and H. M. Crosswhite, Appl. Opt. **2**, 681 (1963).

[24]R. N. Schwartz and R. M. Macfarlane (unpublished).

[25]P. A. M. Berdovsky, M. J. J. Lammers, and G. Blasse, J. Chem. Phys. **83**, 476 (1985).

[26]C. Andraud, F. Pellé, J. P. Denis, O. Pilla, and B. Blanzat, J. Phys.: Condens. Matter **1**, 1511 (1989).